

Extremely large magnetoresistance in single-crystalline $ZrBi_2$

Cundong Li(李存东), Binbin Ruan(阮彬彬), Qingxin Dong(董庆新), Jianli Bai(白建利), Libo Zhang(张黎博), Qiaoyu Liu(刘乔宇), Jingwen Cheng(程靖雯), Pinyu Liu(刘品宇), Yu Huang(黄宇), Yingrui Sun(孙英睿), Zhian Ren(任治安), and Genfu Chen(陈根富)

Citatio: Chin. Phys. B, 2025, 34 (**9**): 097307. DOI: 10.1088/1674-1056/add246
http://cpb.iphy.ac.cn; http://iopscience.iop.org/cpb

What follows is a list of articles you may be interested in

Quantum oscillations in $TaCo_2Te_2$ thin flakes

Ruiyang Jiang(蒋睿阳), Tian Le(乐天), Yunteng Shi(石云腾), Changcun Li(李长存), Xinyi Zheng(郑新义), Xingchen Guo(郭兴宸), Bingbing Tong(仝冰冰), Peiling Li(李沛岭), Ziwei Dou(窦子威), Xiaohui Song(宋小会), Jie Shen(沈洁), Zhaozheng Lyu(吕昭征), Guangtong Liu(刘广同), Fucai Liu(刘富才), Li Lu(吕力), and Fanming Qu(屈凡明)

Chin. Phys. B, 2025, 34 (**8**): 087307. DOI: 10.1088/1674-1056/add5ce

In-plane negative magnetoresistance and quantum oscillations in van der Waals antiferromagnet $DyTe_3$

Qi Qi(齐琦), Senhao Lv(吕森浩), Ke Zhu(祝轲), Yaofeng Xie(谢耀锋), Guojing Hu(胡国静), Zhen Zhao(赵振), Guoyu Xian(冼国裕), Yechao Han(韩烨超), Yang Yang(杨洋), Lihong Bao(鲍丽宏), Xiao Lin(林晓), Hui Guo(郭辉), Haitao Yang(杨海涛), and Hong-Jun Gao(高鸿钧)

Chin. Phys. B, 2025, 34 (**7**): 077305. DOI: 10.1088/1674-1056/adcc87

Magnetic and electrical transport properties in GdAlSi and SmAlGe

Jing Gong(巩静), Huan Wang(王欢), Xiao-Ping Ma(马小平), Xiang-Yu Zeng(曾祥雨), Jun-Fa Lin(林浚发), Kun Han(韩坤), Yi-Ting Wang(王乙婷), and Tian-Long Xia(夏天龙)

Chin. Phys. B, 2024, 33 (**7**): 077302. DOI: 10.1088/1674-1056/ad41ba

Symmetry transformation of nonlinear optical current of tilted Weyl nodes and application to ferromagnetic $MnBi_2Te_4$

Zhuo-Cheng Lu(卢倬成) and Ji Feng(冯济)

Chin. Phys. B, 2024, 33 (**4**): 047303. DOI: 10.1088/1674-1056/ad2bfb

High-resolution angle-resolved photoemission study of large magnetoresistance topological semimetal $CaAl_4$

Xu-Chuan Wu(吴徐传), Shen Xu(徐升), Jian-Feng Zhang(张建丰), Huan Ma(马欢), Kai Liu(刘凯), Tian-Long Xia(夏天龙), and Shan-Cai Wang(王善才)

Chin. Phys. B, 2021, 30 (**9**): 097303. DOI: 10.1088/1674-1056/ac0cd7

Extremely large magnetoresistance in single-crystalline $ZrBi_2$

Cundong Li(李存东)[1,2,†], Binbin Ruan(阮彬彬)[3,†], Qingxin Dong(董庆新)[1,2], Jianli Bai(白建利)[1,2], Libo Zhang(张黎博)[1,2], Qiaoyu Liu(刘乔宇)[1,2], Jingwen Cheng(程靖雯)[1,2], Pinyu Liu(刘品宇)[1,2], Yu Huang(黄宇)[1,2], Yingrui Sun(孙英睿)[1,2], Zhian Ren(任治安)[1,2], and Genfu Chen(陈根富)[1,2,4,‡]

[1] *Institute of Physics and Beijing National Laboratory for Condensed Matter Physics, Chinese Academy of Sciences, Beijing* 100190, *China*
[2] *School of Physical Sciences, University of Chinese Academy of Sciences, Beijing* 100049, *China*
[3] *College of Physics and Center of Quantum Materials and Devices, Chongqing University, Chongqing* 401331, *China*
[4] *Songshan Lake Materials Laboratory, Dongguan* 523808, *China*

(Received 10 March 2025; revised manuscript received 28 April 2025; accepted manuscript online 30 April 2025)

Magnetoresistance (MR) is a pivotal transport phenomenon within the realm of condensed matter physics. In recent years, materials exhibiting extremely large unsaturated magnetoresistance (XMR), which are often potential topological materials, have garnered significant attention. In this study, we synthesized single crystals of $ZrBi_2$ and performed electrical and specific heat measurements on them. The resistivity of $ZrBi_2$ displays metallic behavior with a high residual resistance ratio. Notably, the MR of $ZrBi_2$ reaches approximately 2.0×10^3% at 2 K and 16 T without saturation. Weak Shubnikov–de Haas oscillations with two frequencies were observed above 13.5 T, which correspond to 237 T and 663 T. Hall effect fitting yields nearly equal concentrations of electron and hole carriers with concentrations of approximately 10^{21} cm^{-3} and mobilities of approximately 5000 $cm^2\cdot V^{-1}\cdot s^{-1}$ at 2 K. The XMR could be attributed to the electron–hole compensation with high mobility.

Keywords: extremely large magnetoresistance, SdH oscillation, electron–hole compensation

PACS: 73.43.Qt, 71.70.Di, 72.15.–v, 72.80.Ga

DOI: 10.1088/1674-1056/add246 **CSTR:** 32038.14.CPB.add246

1. Introduction

Magnetoresistance (MR) is defined as the change in resistance of materials under an external magnetic field. In general, in non-magnetic metals the MR is usually only a few per cent, and is referred to as ordinary magnetoresistance. In recent years, extremely large magnetoresistance (XMR) has garnered significant attention. XMR is characterized by a rapid increase in the MR of materials at low temperature, reaching as high as 10^3%–10^8%,[1] and, more importantly, the XMR does not saturate even under extremely high magnetic fields.[1] For instance, the MR of WP_2 can reach 2×10^8% at 63 T without saturation,[2] which is the highest MR ever discovered. Several potential mechanisms have been proposed for XMR, including electron–hole compensation, ultrahigh mobility, a high residual resistance ratio (RRR), topological fermions, steep bands and so on.[1] The electron–hole compensation mechanism is usually considered to be the main mechanism for XMR, but it is not the only source of XMR. Many materials with XMR, such TaAs,[3] NbAs,[4] LaBi[5] and YBi,[6] also exhibit quantum oscillations and possess non-trivial Berry phases, other important mechanisms of XMR. That is due to the presence of linearly dispersive energy bands with very small effective masses and high mobility in the topological material.

Transition metal dichalcogenides (TMDs) are an important family of materials with XMR, for example, $MoTe_2$,[7] WTe_2,[8,9] $HfTe_2$[10] and the Dirac semimetals $PtTe_2$[11,12] and $PdTe_2$.[13] Transition metal dipnictides (TMDPs) are another potential family of materials with XMR. Some examples of nodal line semimetals have been studied in MX_2 TMDPs (M = Nb, Ta, Mo; X = P, As, Sb).[2,14–17] According to the generality of theory based on nonsymmorphic symmetry and incomplete charge transfer, the observation of XMR in TMDPs should be universal.[18,19] However, to our knowledge there are only a few materials with XMR found among the TMDPs. The materials with XMR found in the TMDPs are concentrated in the VB and VIB groups, such as $NbSb_2$,[15] $TaSb_2$,[16] WP_2,[2] and MoP_2.[2] Another example with unsaturated XMR, ZrP_2,[18] complements the above theory but remains understudied. On the other hand, although XBi (X = La, Y, Er, In, etc.)[5,6,20] is another important family of materials with XMR, and the MR of $PtBi_2$ reaches $\sim10^7$%,[21] close to WP_2[2] and WTe_2,[8,9] studies on bismuthides are still insufficient. Since bismuthides usually have strong spin–orbit coupling (SOC), it is expected that XMR or other novel transport phenomena would be exhibited in bismuthides.

Here, we investigate $ZrBi_2$ as a case study in the hope of complementing the group IVB TMDPs. Some preliminary characterization, such as resistivity and specific heat, has

†These authors contributed equally to this work.
‡Corresponding author. E-mail: gfchen@iphy.ac.cn

© 2025 Chinese Physical Society and IOP Publishing Ltd. All rights, including for text and data mining, AI training, and similar technologies, are reserved.

been reported in abstract form at a conference[22] and a MR of 400% (2 K, 9 T) of $ZrBi_2$ with a RRR of 30 has also been reported.[23] Like other TMDs and TMDPs, $ZrBi_2$ exhibits metallic behavior with a high RRR of approximately 60, which is significantly higher than in the early investigations, and has a resistivity plateau in an external magnetic field. At 2 K and 16 T, the MR of $ZrBi_2$ reaches $\sim 2.0 \times 10^3$% without saturation and exhibits Shubnikov–de Haas (SdH) oscillations with two oscillation frequencies. The Hall effect suggests that the concentrations of electron and hole carriers are close to each other and the high mobilities of both carriers are close to 5000 $cm^2 \cdot V^{-1} \cdot s^{-1}$. Therefore, the XMR of $ZrBi_2$ originates from electron–hole compensation and high mobility. The energy band structure calculated from first principles suggests strong SOC in $ZrBi_2$.

2. Methods

Single crystals of $ZrBi_2$ were grown by Bi flux. The starting reactants, including Zr powder (99.9%) and Bi powder (99.997%), were mixed in a molar ratio of Zr:Bi = 1:10, loaded into an alumina crucible and then sealed into an evacuated quartz tube. The quartz tube was heated to 1073 K, held at this temperature for 20 h and then slowly cooled to 773 K at a rate of 2 $K \cdot h^{-1}$. At this temperature, the flux was removed by centrifugation. The obtained single crystals had a needle-like form with a size of approximately 2 mm × 0.01 mm × 0.01 mm, as shown in Fig. 1(b). The atomic proportions were checked by Oxford X-Max energy dispersive x-ray spectroscopy (EDX) analysis in a Hitachi S-4800 electron microscope. Electrical transport and specific heat measurements on $ZrBi_2$ single crystals were performed on a Quantum Design physical properties measurement system (PPMS-9T and PPMS-16T). Calculations based on first-principles were carried out by the Quantum ESPRESSO package. Projector augmented wave pseudopotentials based on the exchange–correlation functionals of PBEsol were used.[24] We used a Monkhorst–Pack grid of $5 \times 3 \times 13$ in the self-consistent calculations.[25,26] The energy cutoffs for wavefunctions and charge densities were 70 Ry and 600 Ry, respectively.

3. Results and discussion

3.1. Crystal structure

$ZrBi_2$ crystallizes in the nonsymmorphic space group *Pnnm* (No. 58) with lattice parameters $a = 10.18$ Å, $b = 15.49$ Å and $c = 3.971$ Å, belonging to the orthogonal crystal system. Zr atoms and Bi atoms are interconnected and grow along the *c*-axis as shown in Fig. 1(a). Most known TMDPs crystallize either in a MoP_2 structure (space group $Cmc2_1$, No. 36) or an $OsGe_2$ structure (space group $C2/m$, No. 12).[19] The structure of $ZrBi_2$ is distinctly different from other materials but resembles that of ZrP_2, with the same symmetric operation *n* glide plane. The EDX pattern is shown in Fig. 1(c) with a scanning electron microscope (SEM) photograph shown in the inset. The EDX results show an approximate atomic ratio of Zr:Bi = 1:2, suggesting a high-quality single crystal.

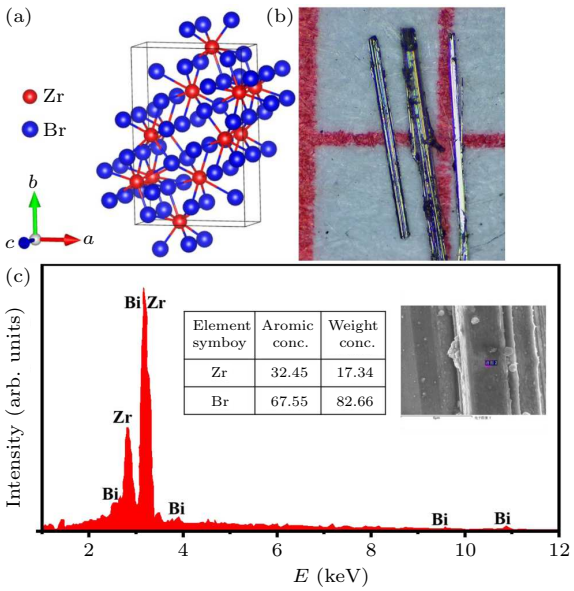


Fig. 1. (a) The structure of $ZrBi_2$. (b) Photograph of single crystals. (c) EDX pattern of $ZrBi_2$ (the inset shows a SEM photograph of $ZrBi_2$).

3.2. Resistivity and MR

The resistivity of $ZrBi_2$ was measured using the standard four-probe method. The temperature-dependent resistivity, $\rho_{xx}(T)$, of $ZrBi_2$ under different external magnetic fields is shown in Fig. 2(a) and its inset. The current is parallel to the direction of the rod, while the direction of the magnetic field is perpendicular to the current. $\rho_{xx}(T)$ at 0 T exhibits metallic behavior with a low residual resistivity of 2.54 μΩ·cm at 2 K, which is of the same order of magnitude as that of other materials with XMR.[8,15] The high RRR [RRR = $\rho_{xx}(300\ \mathrm{K})/\rho_{xx}(2\ \mathrm{K})$] of approximately 57 indicates the good quality of the crystals. Such a high RRR is significantly greater than that of ordinary metals and is a typical feature of materials with XMR.[9,18] The scattering mechanism in the ground state of a material can initially be analyzed using the power-law equation $\rho_{xx}(T) = \rho_0 + aT^n$,[27] and the inset in Fig. 2(a) shows the fitting results for the low-temperature (2–40 K) resistivity at zero field. This fitting yields $\rho_0 = 2.47$ μΩ·cm and $n = 2.4$, close to an integer 2. The fitting result for *n* suggests that the scattering mechanism of $ZrBi_2$ arises from the combination of electron–electron interactions and another weak interaction. At low temperatures below 50 K and high magnetic fields above 6 T a field-induced metal-to-insulator-like transition is observed, as shown in the inset of Fig. 2(a). Such resistivity plateaus are also a typical feature of materials with XMR.

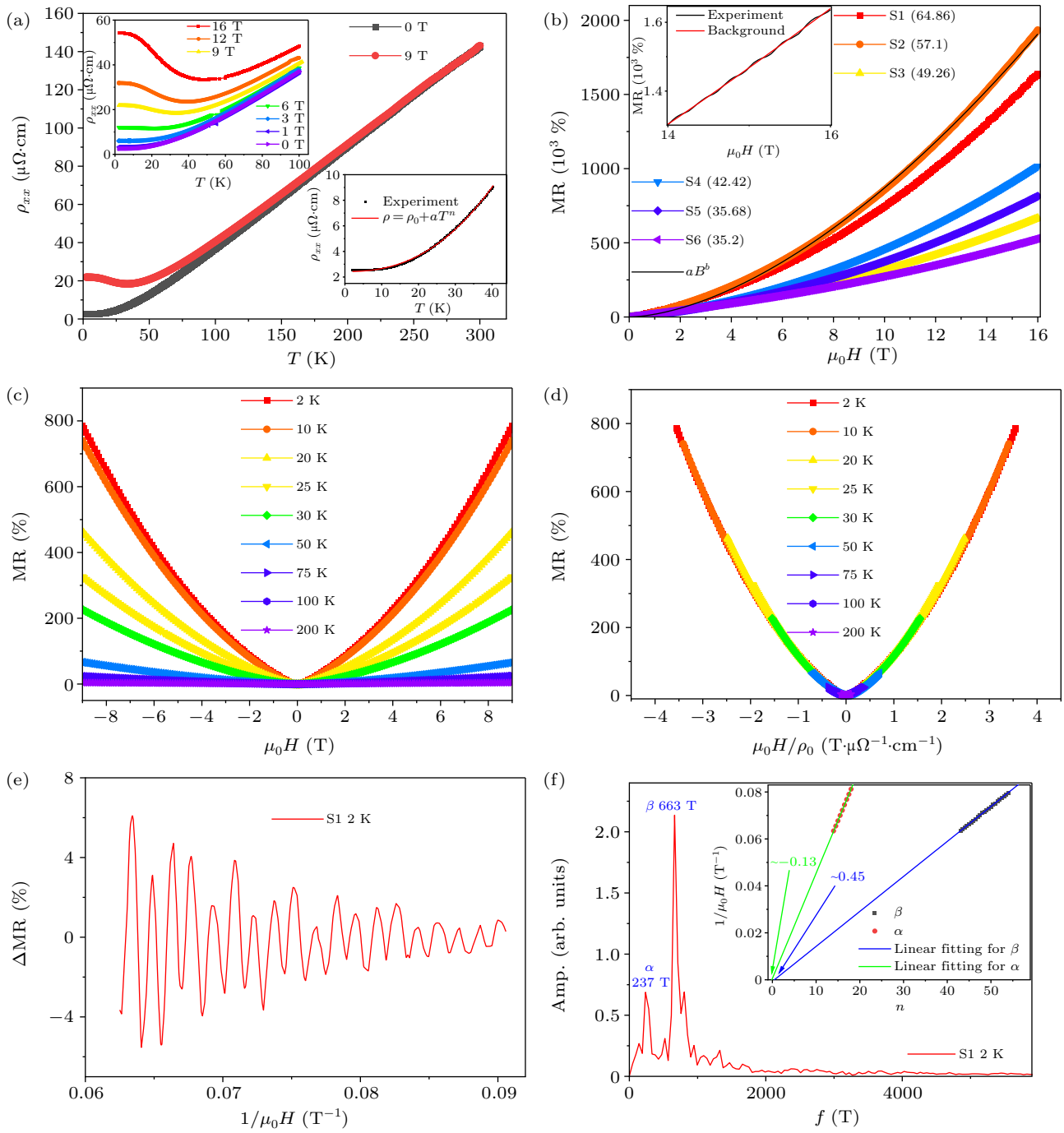


Fig. 2. (a) The resistivity of $ZrBi_2$ at 0 T and 9 T at 2–300 K. The blue solid line is the fitting results of the BG model. The insets are resistivity of $ZrBi_2$ at various fields and the fitting results for $ZrBi_2$ at 2–40 K, respectively. (b) The MR of some samples with different $\mu_0 H$ in the field range of 0–16 T. The inset is the oscillation in sample S1. (c) The MR of sample S2 in the field range ±9 T at various temperatures. (d) The Kohler diagram of MR. (e) The SdH oscillations of MR in sample S1. (f) The results of FFT. The inset is the LL diagram of two oscillations.

At 2 K and at 16 T, the MR ($= [\rho(\mu_0 H) - \rho(0\ \mathrm{T})]/\rho(0\ \mathrm{T}) \times 100\%$) of $ZrBi_2$ reaches $2.0 \times 10^3\%$ and remains unsaturated, as shown in Fig. 2(b). Similar to other materials with XMR, the MR of $ZrBi_2$ is correlated with the quality of the sample.[28] The MR of six samples with different RRRs is shown in Fig. 2(b). However, some samples with a higher RRR exhibit a lower MR (e.g., S3), which may be due to the anisotropy of the MR as discussed below. Although the MR of $ZrBi_2$ is about one order of magnitude lower than that of most materials with XMR, it is close to that of $HfTe_2$[10] and $NiTe_2$[29] and exceeds T_d-$MoTe_2$,[7] $PdTe_2$[13] and CrP.[30]

Notably, weak SdH oscillation with two oscillation frequencies was observed in sample S1 (RRR = 64.86) above 13.5 T, and there is an extremely weak oscillation in sample S2 (RRR = 51.1). However, similar oscillations were not observed in other samples, suggesting the correlation of signal to sample quality. The oscillations are so weak, with ΔMR no more than 6%, that is not noticeable below 16 T. After subtracting a smooth background, as shown in the inset of Fig. 2(b), the oscillation component of MR against the recipro-

cal of the field $1/\mu_0 H$ is shown in Fig. 2(e). Two frequencies, $f_\alpha = 237$ T and $f_\beta = 663$ T, can be identified from the fast Fourier transform (FFT) spectra, as shown in Fig. 2(f). According to the Onsager relation $F = (\hbar/2\pi e)A_F$,[31] the cross-sectional area A_F and the averaged Fermi vector k_F of the corresponding Fermi surface can be estimated as $A_{F-\alpha} = 2.27 \times 10^{-2}$ Å^{-2}, $k_{F-\alpha} = 0.084$ Å^{-1} and $A_{F-\beta} = 6.4 \times 10^{-2}$ Å^{-2}, $k_{F-\beta} = 0.14$ Å^{-1}. SdH oscillations are also an efficient method for recognizing the Berry phase according to the Lifshitz–Onsager quantization rule[31]

$$\frac{F}{B} = n + \frac{1}{2} - \frac{\phi_B}{2\pi} - \delta = n + \frac{1}{2} - \beta - \delta, \tag{1}$$

where ϕ_B is the Berry phase and δ is a phase offset-related Fermi surface curvature which always has a value of $\pm 1/8$ in a 3D case. The Landau level (LL) index fan diagram is shown in the inset of Fig. 2(f). The integer indices and half-integer indices are assigned to be the maxima and minima of ΔMR, respectively. A linear fitting of the index plot gives a slope of 0.00448 T^{-1} for f_α and 0.00149 T^{-1} for f_β. The intercepts of linear extrapolation are -0.13 for f_α and 0.45 for f_β, thus the calculated Berry phases are 0.74π for f_α and 1.9π for f_β. These two Berry phases are given with $\delta = 0$ since the types of carriers corresponding to the two oscillation frequencies could not be determined. However, since the oscillation is weak and far from the quantum limit, such results may be subject to error and further experiments and theoretical calculations are necessary.

Figure 2(c) displays the field-dependent MR of sample S2 at various temperatures, with the field ranging from -9 T to 9 T. The MR of $ZrBi_2$ reaches 785% at 2 K and 9 T and the MR becomes progressively smaller as the temperature increases. According to Kohler's law,[32–34] for a single-carrier or two-carrier exactly compensated system the MR at different temperatures should satisfy the same function

$$\mathrm{MR} \propto \left(\frac{\mu_0 H}{\rho_0}\right)^m, \tag{2}$$

where m is a constant. As shown in Fig. 2(d), the MR of $ZrBi_2$ at various temperatures can be scaled onto a single line with the horizontal coordinate $\mu_0 H/\rho_0$. Considering the Hall effect discussed below, the MR following Kohler's law suggests that there are two carriers with nearly complete compensation in $ZrBi_2$. However, materials whose MR satisfies Kohler's law over a large temperature range are not common, meaning that the carriers compensate in the 2–200 K range. According to the semiclassical Drude model, for materials with fully compensated electron and hole carriers, the MR should follow $\mathrm{MR} \propto \mu_e \mu_h B^2$.[35] The fitting results for $\mathrm{MR} = aB^b$ are shown in the Fig. 1(b), and the index obtained is $b = 1.7$. The index is slightly less than 2 and it is common in many materials in which electrons and holes are not exactly compensated.[34]

3.3. Angular MR

To confirm the symmetry of the MR in $ZrBi_2$, the angle-dependent MR was characterized. As shown in Fig. 3(a), the current is parallel to the direction of the rod, while the direction of the magnetic field rotates around the axis perpendicular to the current. The maximum value of MR ($\sim 780\%$) occurs when B is perpendicular to I and the minimum value of MR (~ 0) occurs when B is parallel to I, as shown in the inset of Fig. 3(b). As shown in Fig. 3(b), MR decreases as the angle changes, and it exhibits a twofold symmetry within one period. However, no negative MR was found. Since the negative MR due to chiral anomalies is highly sensitive to the angle and can easily disappear with small deviations,[3] it is possible that the lack of observed negative MR is due to the fact that B is not strictly parallel to I.

Further, another angle-dependent MR of sample S7 (RRR = 50) was characterized, as shown in Fig. 3(c). The current is parallel to the direction of the rod, while the direction of the magnetic field rotates around the direction of the current. The MR also exhibits a twofold symmetry since the crystal structure of $ZrBi_2$ has a twofold symmetry. As shown in Fig. 3(d), the maximum value of MR ($\sim 520\%$) occurs at $\varphi \approx 56^\circ$ and the minimum value of MR ($\sim 80\%$) occurs at $\varphi \approx 147^\circ$. These results indicate that the MR of $ZrBi_2$ is strongly anisotropic. Therefore, the lower MR of samples with a higher RRR may have its origins in this anisotropy.

3.4. Hall effect

Figure 4(a) displays the magnetic field-dependent Hall resistivity of $ZrBi_2$ at various temperatures. The Hall resistivity bends slightly at low fields, deviating from linear behavior, suggesting the nature of a double band. According to the double-band model,[36] the Hall conductivity tensor is given by

$$\sigma_{xy} = \frac{\rho_{xy}}{\rho_{xy}^2 + \rho_{xx}^2}, \tag{3}$$

$$\sigma_{xy} = eB\left[\frac{n_h \mu_h^2}{1 + (\mu_h B)^2} - \frac{n_e \mu_e^2}{1 + (\mu_e B)^2}\right], \tag{4}$$

where n_e (n_h) and μ_e (μ_h) are the concentration and mobility of the electron (hole) carriers, respectively. The conductivity σ_{xy} is shown in Fig. 4(b). The concentrations and mobilities of the electron and hole carriers, obtained by fitting Eq. (4), are presented in Figs. 4(c) and 4(d), respectively. The concentration of both carriers is approximately 10^{21} cm^{-3}, which is common in semimetal materials[12,21] and higher than that in ZrP_2.[18] The mobilities of both carriers are in the range of 1000–5000 cm^2·V^{-1}·s^{-1}. The concentration and the mobility of the carriers do not vary much over the measuring range. The difference between the electron carrier concentration and

the hole carrier concentration is very small, and the mobility remains almost unchanged. The maximum value of the ratio of the electron carrier concentration to the hole carrier concentration occurs at $T = 2$ K, and is less than 1.2; the ratio at high temperatures is always between 1 and 1.1. Therefore, the XMR of $ZrBi_2$ is the origin of the electron–hole compensation and the high mobility,[18] which is also consistent with previous discussions.

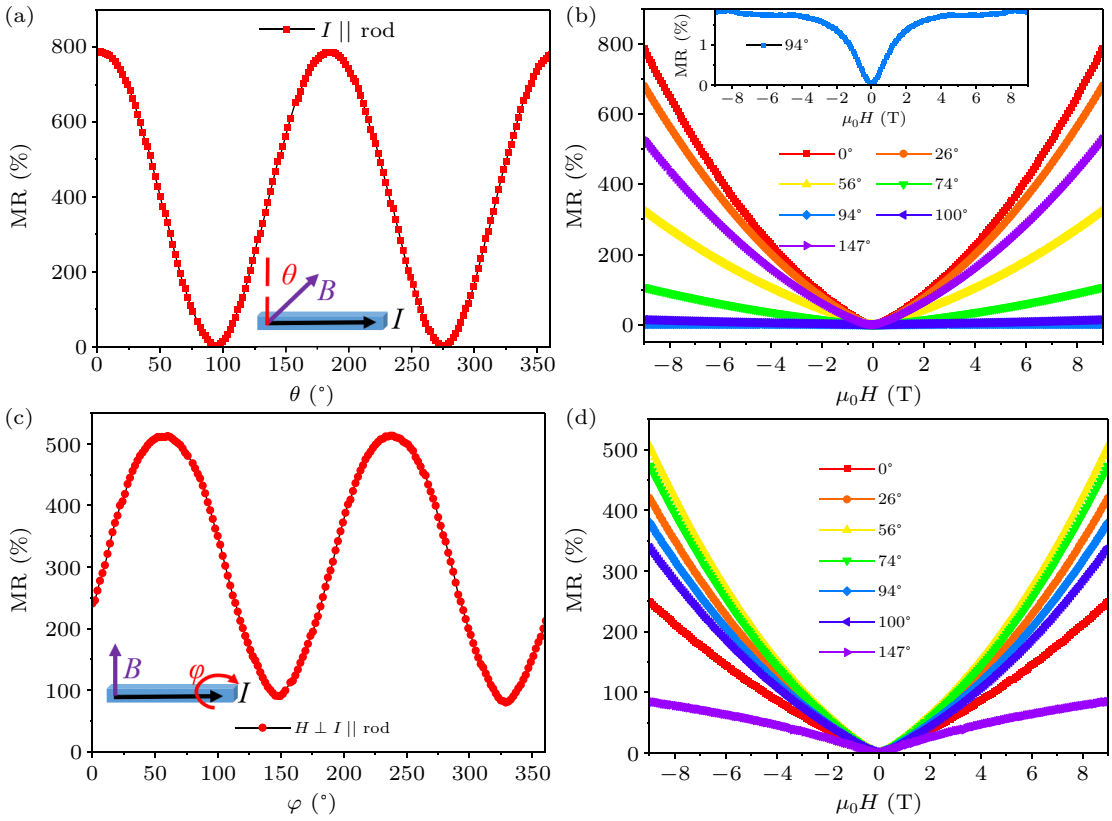


Fig. 3. (a) Angle-dependent MR of $ZrBi_2$ (the direction is shown in the inset). (b) The MR at different angles θ. (c) Angle-dependent MR of $ZrBi_2$ (the direction is shown in the inset). (d) The MR at different angles φ.

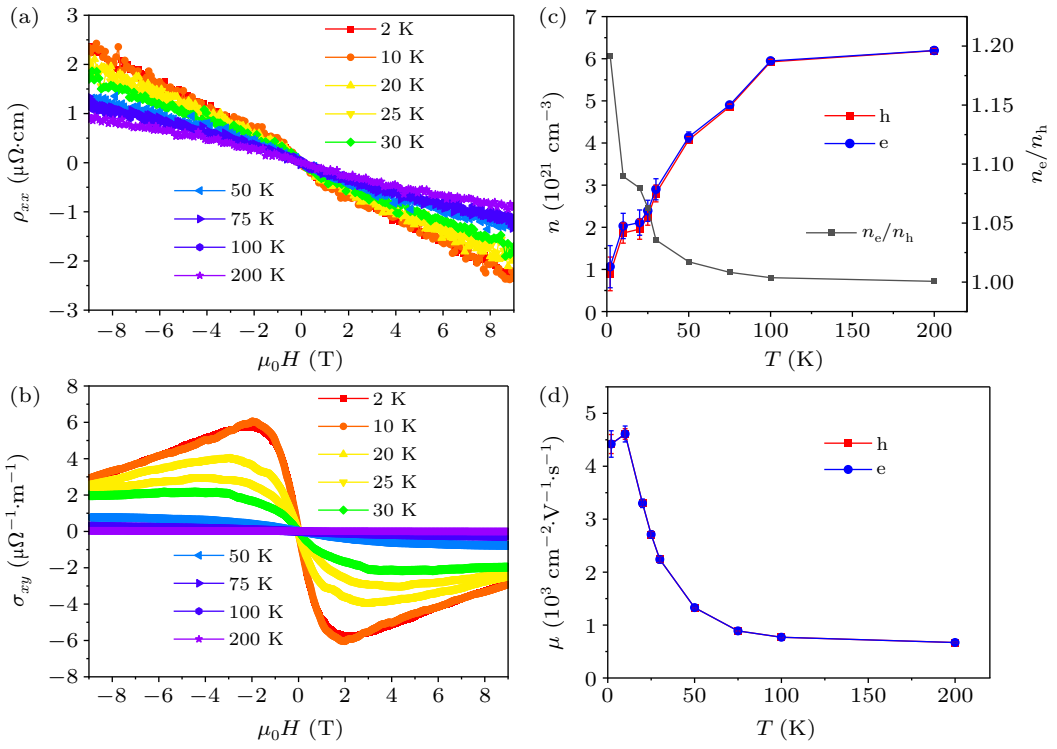


Fig. 4. (a) The Hall resistivity of $ZrBi_2$ at various temperatures. (b) The Hall conductivity of $ZrBi_2$. (c) and (d) The concentration and mobility of electron carriers and hole carriers, respectively.

3.5. Specific heat

Figure 5 displays the specific heat measurements for a single crystal of $ZrBi_2$; there is no significant transition in the measurement range of 2–200 K, which indicates the absence of phase transitions in $ZrBi_2$. The specific heat can be described by the Debye model $C(T) = \gamma T + \beta T^3$, and the inset to Fig. 5 shows the fitting results for the temperature range 2.5–10 K. The fitting yields $\beta = 1.26$ mJ·mol^{-1}·K^{-4} and $\gamma = 9.21$ mJ·mol^{-1}·K^{-2}, and the Debye temperature Θ_D can be calculated using the formula $\Theta_D = [12\pi^4 NR/(5\beta)]^{1/3}$. This calculation gives $\Theta_D = 166.6$ K.

3.6. Band structure

To better understand $ZrBi_2$, the electronic structures of $ZrBi_2$ with or without SOC are calculated via first-principles calculations. Figures 6(a) and 6(c) display the calculated band structures and the density of states (DOS) without SOC, respectively. Obviously, several energy bands across the Fermi level result in several Fermi pockets, including both hole-type and electron-type Fermi pockets. No signatures of any Dirac fermions or Weyl fermions are observed in the energy band structure, so that $ZrBi_2$ may be a trivial metal. The energy bands near the Fermi surface are mainly composed of p-orbitals for Bi atoms and d-orbitals for Zr atoms. Figures 6(b) and 6(d) show the calculated band structures and the DOS considering SOC, respectively. SOC introduces energy band splitting along the high-symmetry lines, such as Z–U, R–T and X–U. In addition, SOC increases the DOS on the Fermi level. These results suggest that the SOC effects in $ZrBi_2$ are significant, which is as expected for the heavy atom Bi.

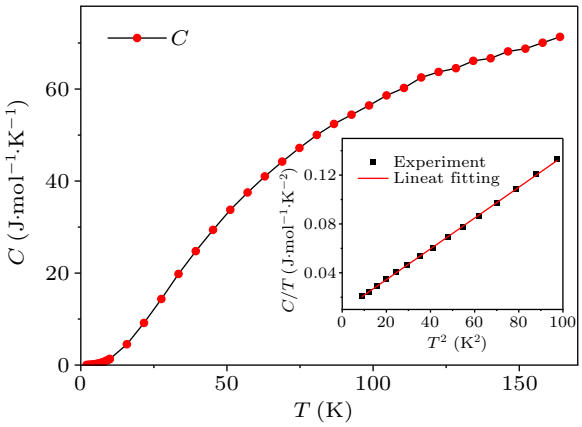


Fig. 5. The specific heat of $ZrBi_2$. The inset shows the fitting results by the Debye model.

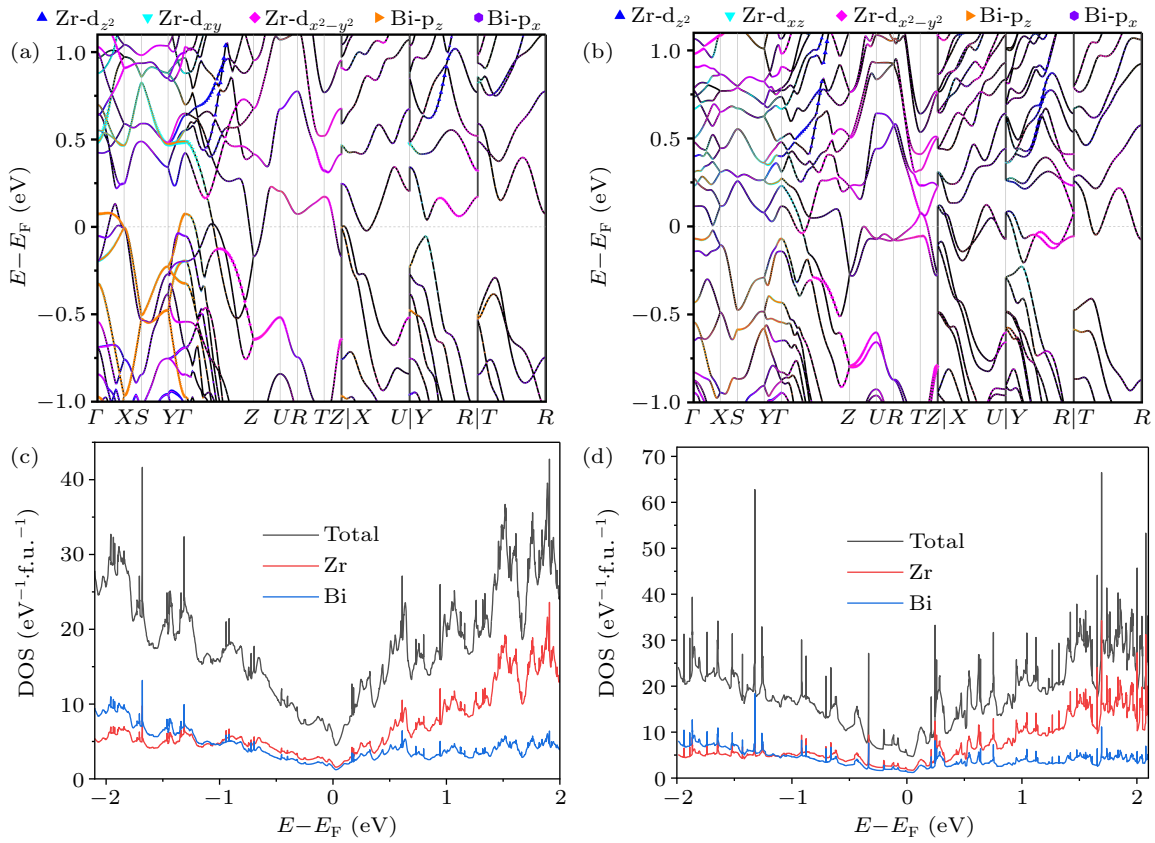


Fig. 6. (a) and (b) Band structure of $ZrBi_2$ with and without SOC, respectively. (c) and (d) DOS of $ZrBi_2$ with and without SOC, respectively.

4. Conclusion

In conclusion, we have synthesized high-quality single crystals of $ZrBi_2$ and performed comprehensive electrical and thermal measurements on them. $ZrBi_2$ crystallizes in a non-symmorphic space group and forms needle-like single crystals. The resistivity of $ZrBi_2$ exhibits metallic behavior with

a high RRR of approximately 60. The extremely large MR of $ZrBi_2$ reaches approximately 2.0×10^3% at 2 K and 16 T without saturation. SdH oscillations with the two frequencies of 237 T and 663 T are observed. Both Kohler's law and the Hall effect suggest that the electrons and holes in $ZrBi_2$ are nearly perfectly compensated. The XMR of $ZrBi_2$ is the origin of the electron–hole compensation and high mobility. The calculation of $ZrBi_2$ based on first-principles suggests that the states near the Fermi level are mainly composed of p-orbitals for Bi atoms and d-orbitals for Zr atoms and $ZrBi_2$ has strong SOC.

Acknowledgments

Project supported by the National Natural Science Foundation of China (Grant No. 12274440), the National Key R&D Program of China (Grant No. 2022YFA1403903), and the Synergetic Extreme Condition User Facility (SECUF).

References

[1] Niu R and Zhu W K 2021 *J. Phys. Condens. Matter* **34** 113001
[2] Kumar N, Sun Y, Xu N, Wang P, Zhang D, Ding W, Liu K, Law K T, Zeng Y J, Shen B and Yan B 2017 *Nat. Commun.* **8** 1642
[3] Huang X, Zhao L, Long Y, Wang P, Chen D, Yang Z, Liang H, Xue M, Weng H, Fang Z, Dai X and Chen G 2015 *Phys. Rev. X* **5** 031023
[4] Luo Y, Ghimire N J, Wartenbe M, Choi H, Neupane M, McDonald R D, Zhu J, Bauer E D, Ronning F and Thompson J D 2015 *Phys. Rev. B* **92** 205134
[5] Kumar N, Shekhar C, Wu S C, Le C, Schmidt H, Borrmann H, Yan B, Parkin S S P, Felser C and Yan B 2016 *Phys. Rev. B* **93** 241106
[6] Qian B, Tang F, Ruan Y R, Wu D, Chen J, Zhou L, Gao Y, Chen X, Liu J and Guo Y 2018 *J. Mater. Chem. C* **6** 10020
[7] Lv Y Y, Li X, Pang B, Lin S, Luo X, Chen G, Luo J, Han F, Zhu W and Wang W 2017 *J. Appl. Phys.* **122** 045102
[8] Ali M N, Xiong J, Flynn S, Tao J, Gibson Q D, Schoop L M, Liang T, Haldolaarachchige N, Hirschberger M, Ong N P and Cava R J 2014 *Nature* **514** 205
[9] Wang Y, Wang L, Liu X, Zhang H, Wang H, Zhao L, Li X, Dai X, Liu X, Chen G and Wang N 2019 *Nano Lett.* **19** 3969
[10] Mangelsen S, Naumov P G, Barkalov O I, Palasyuk T, Medvedev S A, Schwarz U, Hanfland M, Tsirlin A A and Grin Y 2017 *Phys. Rev. B* **96** 205148
[11] Zheng W, Schönemann R, Aryal N, Zhou Q, Rhodes D, Chikara S, Balicas L, Siegrist T and Manousakis E 2018 *Phys. Rev. B* **97** 235154
[12] Pavlosiuk O and Kaczorowski D 2018 *Sci. Rep.* **8** 11297
[13] Wang Y, Zhang J, Zhu W, Zhang Y, Weng H, Zhang W, Yang L, Liu Z, Feng S, Zhao X, Li X, Dai X, Fang Z and Chen G 2016 *Sci. Rep.* **6** 31554
[14] Shao Y, Sun Z, Wang Y, Li D, Pi L, Lu X, Zhao Y, Zhang W, Chen Y, Zhou S and Zhang Y 2018 *Proc. Natl. Acad. Sci. USA* **116** 1168
[15] Wang K, Graf D, Li L, Wang L and Petrovic C 2014 *Sci. Rep.* **4** 7328
[16] Li Y, Li L, Wang J, Li T, Chen G, Luo J, Han F, Zhu W and Wang W 2016 *Phys. Rev. B* **94** 121115
[17] Leahy I A, Lin Y P, Siegfried P E, Graf D, Tien H J and Lee Y S 2018 *Proc. Natl. Acad. Sci. USA* **115** 10570
[18] Bannies J, Razzoli E, Michiardi M, Boschini F, Zwartsenberg B, Day R P, Elfimov I S, Damascelli A, Denlinger J D, Yang L X, Sobota J A, Rotenberg E, Frandsen B A, Cheung S C, Birgeneau R J and Elfimov I 2021 *Phys. Rev. B* **103** 155144
[19] Hulliger F 1964 *Nature* **204** 775
[20] Okawa K, Kanou M, Namiki H, Ishii H, Murakawa H, Hanaguri T and Sasagawa T 2018 *Phys. Rev. Mater.* **2** 124201
[21] Gao W, Hao N, Zheng F W, Ma X, Zhou P, Zhang Y, Lu P, Zhang J, Yang J, Singh D J, Zhang L and Wang L 2017 *Phys. Rev. Lett.* **118** 256601
[22] Sobczak Z, Winiarski M J, Kolincio K, Klimczuk T and Kaczorowski D 2017 *Cryst. Growth Des.* **17** 6016
[23] Han T 2017 *The Transport Study of Strong Spin Orbit Coupling Material of Sr_2IrO_4 and $ZrBi_2$* (University of Science and Technology of China)
[24] Giannozzi P, Baroni S, Bonini N, *et al.* 2009 *J. Phys. Condens. Matter* **21** 395502
[25] Giannozzi P, Andreussi O, Brumme T, *et al.* 2017 *J. Phys. Condens. Matter* **29** 465901
[26] Perdew J P, Ruzsinszky A, Csonka G I, Vydrov O A, Scuseria G E, Constantin L A, Zhou X and Burke K 2008 *Phys. Rev. Lett.* **100** 136406
[27] M Z J 2001 *Electrons and Phonons: The theory of transport phenomena in solids* (New York: Oxford University Press)
[28] Gong J X, Yang J, Ge M, Liu Y, Luo X, Chen G, Luo J, Han F, Zhu W and Wang W 2018 *Chin. Phys. Lett.* **35** 097101
[29] Xu C, Li B, Jiao W, Zhou W, Qian B, Sankar R, Chou F C, Lin H, Liu Z, Chen Y and Wang N 2018 *Chem. Mater.* **30** 4823
[30] Niu Q, Yu W C, Aulestia E I P, Cheung S K Y, Wong C H, Yang S A and Lin H 2019 *Phys. Rev. B* **99** 125126
[31] Murakawa H, Bahramy M S, Tokunaga M, Kohmoto Y, Nagaosa N and Tokura Y 2013 *Science* **342** 1490
[32] Nie L, Luo G and Koh H 2002 *Physica C* **371** 259
[33] Kohler M 1938 *Ann. Phys.* **424** 211
[34] Xu J, Han F, Wang T T, Wang X, Liu Y, Chen G, Luo J, Zhu W and Wang W 2021 *Phys. Rev. X* **11** 041029
[35] Zhao L, Xu Q, Wang X, Xia B, Dai X, Chen G, Luo J, Han F, Zhu W and Wang W 2017 *Phys. Rev. B* **95** 115119
[36] Xia B, Ren P, Sulaev A, Liu P, Shen S Q and Wang L 2013 *Phys. Rev. B* **87** 085442